
Faculty Scholarship

5-5-2023

Microwave Regeneration and Thermal and Oxidative Stability of Imidazolium Cyanopyrrolide Ionic Liquid for Direct Air Capture of Carbon Dioxide

Yun-Yang Lee

Case Western Reserve University

Eda Cagli

Case Western Reserve University, exc508@case.edu

Aidan Klemm

Case Western Reserve University, ajk170@case.edu

Ruth Dikki

Case Western Reserve University, rcd82@case.edu

Author(s) ORCID Identifier:

 Yun-Yang Lee

 Aidan Klemm

 Burcu Gurkan

Follow this and additional works at: <https://commons.case.edu/facultyworks>

 Part of the [Chemical Engineering Commons](#), and the [Chemistry Commons](#)

Recommended Citation

Y.-Y. Lee, E. Cagli, A. Klemm, Y. Park, R. Dikki, M. K. Kidder, B. Gurkan. Microwave Regeneration and Thermal and Oxidative Stability of Imidazolium Cyanopyrrolide Ionic Liquid for Direct Air Capture of Carbon Dioxide. *ChemSusChem* 2023, 16, e202300118.

This Article is brought to you for free and open access by Scholarly Commons @ Case Western Reserve University. It has been accepted for inclusion in Faculty Scholarship by an authorized administrator of Scholarly Commons @ Case Western Reserve University. For more information, please contact digitalcommons@case.edu.

Microwave Regeneration and Thermal and Oxidative Stability of Imidazolium Cyanopyrrolide Ionic Liquid for Direct Air Capture of Carbon Dioxide

Yun-Yang Lee^{+, [a]}, Eda Cagli^{+, [a]}, Aidan Klemm,^[a] Yensil Park,^[b] Ruth Dikki,^[a] Michelle K. Kidder,^[b] and Burcu Gurkan^{*[a]}

Understanding the oxidative and thermal degradation of CO₂ sorbents is essential for assessing long-term sorbent stability in direct air capture (DAC). The potential degradation pathway of imidazolium cyanopyrrolide, an ionic liquid (IL) functionalized for superior CO₂ capacity and selectivity, is evaluated under accelerated degradation conditions to elucidate the secondary reactions that can occur during repetitive absorption-desorption thermal-swing cycles. The combined analysis from various spectroscopic, chromatographic, and thermal gravimetric meas-

urements indicated that radical and S_N2 mechanisms in degradation are encouraged by the nucleophilicity of the anion. Thickening of the liquid and gas evolution are accompanied by 50% reduction in CO₂ capacity after a 7-day exposure to O₂ under 80 °C. To prevent long exposure to conventional thermal heating, microwave (MW) regeneration of the CO₂-reactive IL is used, where dielectric heating at 80 and 100 °C rapidly desorbs CO₂ and regenerates the IL without any measurable degradation.

Introduction

Ionic liquids (ILs) are salts that are commonly liquid under ambient conditions. Made mostly of bulky organic ions, ILs have almost infinite structural and chemical tunability. They are often referred to as “green solvents” or “designer solvents” for their intrinsic physicochemical properties, such as negligible volatility, non-flammability, good thermal stability, as well as wide electrochemical window.^[1–5] ILs demonstrate unique features for a broad spectrum of applications, such as media for synthesis, electrolytes, lubricants, as well as gas separations.^[5–11] Specifically, the low volatility and high CO₂ solubility of ILs are appealing in CO₂ separations. CO₂ occupies the intrinsic entropic voids of ILs through the distinctive interactions between the quadrupolar CO₂ and polar ions.^[12] Furthermore, ILs can be functionalized with nucleophilic functionalities that chemically bind with CO₂.^[13] IL based sorbents, with amine,^[14–20] strong base,^[21,22] and multiple site cooperative interactions,^[23,24] have been extensively studied for post combustion carbon capture and more recently considered for direct air capture


(DAC). The distinct environmental difference in DAC from post combustion capture is the presence of significant amount of O₂ in air. Thermal and oxidative stability is important for the longevity and recyclability of materials for DAC^[25,26] and the behavior of ILs is not well known, particularly those that are being developed for DAC.


In addition to the importance of thermal and oxidative stability, regenerability with precise energy regulation and with external stimuli are of interest for CO₂ capture sorbents. Regeneration of sorbents has traditionally relied on temperature-swing operations and the availability of thermal energy to desorb the CO₂ and recycle the sorbent.^[26,27] Recently, bottom-up approaches involving metal-ion coordinated amines as reactive CO₂ capture agents are demonstrated to lower the energy requirement and increase sorbent stability for regeneration.^[28] With the increasing availability of renewable energy sources, alternative regeneration approaches that do not rely on thermal energy from fossil-fuel burning is gaining interest. There have been few reports on the microwave-based regeneration of conventional aqueous amines^[29,30] and solid sorbents.^[31–33] However, it is not known whether ILs are susceptible to this emerging regeneration approach. Recognizing that electromagnetic field has heating effects that originate from conduction and dielectric polarization phenomena,^[34,35] we postulate that ILs with high concentrations of charged species would be ideal liquid candidates for dielectric heating. Highly polar materials are susceptible to dielectric heating as the alternating electric field at MW frequency range causes the dipoles to reorient in an oscillatory fashion, the friction of which generates heat.^[35] Furthermore, it is expected that the energy would be more intense and targeted than direct thermal heating for the CO₂-rich domains of functionalized ILs since CO₂-bound species are ionic (i.e., carbamate, carboxylate, carbonate).^[30]

[a] Dr. Y.-Y. Lee,⁺ Dr. E. Cagli,⁺ A. Klemm, R. Dikki, Prof. B. Gurkan
Department of Chemical and Biomolecular Engineering
Case Western Reserve University
10900 Euclid Ave, Cleveland, OH, 44106 (USA)
E-mail: beg23@case.edu

[b] Dr. Y. Park, Dr. M. K. Kidder
Energy Science and Technology Directorate
Oak Ridge National Laboratory
1 Bethel Valley Rd., Bldg. 5800, Oak Ridge, TN, 37830 (USA)

[⁺] These authors contributed equally to this work.

 Supporting information for this article is available on the WWW under <https://doi.org/10.1002/cssc.202300118>

 © 2023 The Authors. ChemSusChem published by Wiley-VCH GmbH. This is an open access article under the terms of the Creative Commons Attribution License, which permits use, distribution and reproduction in any medium, provided the original work is properly cited.

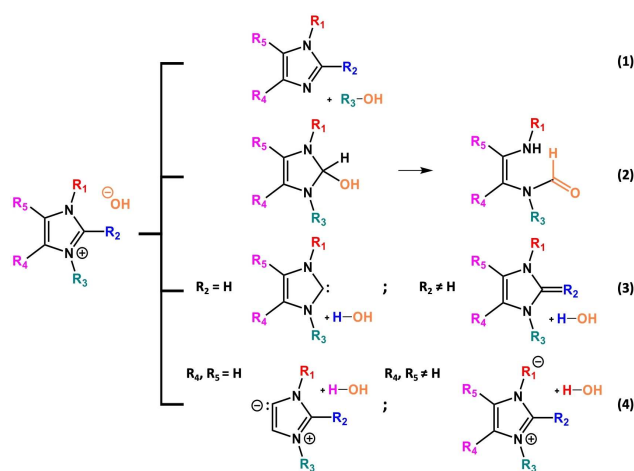
In this study, we addressed the specific knowledge gap on thermal and oxidative stability of a functionalized IL and examined the possibility of microwave regeneration as an alternative to conventional thermal heating. Among the functionalized ILs, 1-ethyl-3-methylimidazolium 2-cyanopyrrolide ([EMIM][2-CNpyr]) has a superior CO₂ capacity, especially under low partial pressures of CO₂.^[36–38] With an effective reaction enthalpy of -50 kJ mole^{-1} , compared to aqueous amine-based sorbents at -80 kJ mole^{-1} , [EMIM][2-CNpyr] can be easily regenerated at mild temperatures (40 °C in anhydrous conditions),^[30] similar is true for the eutectic solvent based on this IL and ethylene glycol.^[29] Under moisture saturated conditions, further increase in temperature is needed (e.g., 90 °C). Therefore, it is important to understand the stability of these solvents upon repetitive absorption-desorption cycles and under exposure to air and oxygen, in particular for DAC processes. Due to its importance in CO₂ capture, the stability of [EMIM][2-CNpyr] under thermal and oxidative conditions as well as exposure to microwaves is examined here to guide the development of future liquid sorbents amenable to various regeneration approaches. In the subsequent paragraphs, we provide the current understanding of the thermal stability and degradation of imidazolium based ILs with the specific techniques applied to date. It is known that the degradation of imidazolium ILs may follow different mechanistic pathways under thermal and/or oxidative environments, depending on their anion pair.^[39–41] Therefore, the known degradation pathways for pyrrole-based compounds are also discussed.

The decomposition of ILs is commonly investigated using thermal gravimetric analysis (TGA) where a fast temperature ramp (e.g., $10 \text{ }^\circ\text{C min}^{-1}$) is applied usually under nitrogen and the degradation is reported based on the observation of significant mass loss.^[42] Recently, there has been improved methods for predicting long-term thermal stability via TGA by the control of furnace parameters.^[43] Ngo et al.^[39] and Baranyai et al.^[44] examined the thermal degradation of [EMIM][TFSI], a common IL, under air and O₂ environments where a decomposition at a lower temperature was observed, compared to the N₂ environment. Few studies^[45,46] examined thermal degradation under isothermal conditions where lower thermal degradation temperatures were determined compared to the temperature ramping method in TGA. Minami et al.^[46] measured close to 10 wt.% mass loss when [EMIM][TFSI] was maintained at 200 °C for 1000 h under air. Further, when the ethyl chain was replaced by a hexyl on the cation, the weight loss under same conditions increased to more than 10 wt.%, thus showing the negative impact of the alkyl length attached to imidazolium on thermal stability. They also observed similar results with Rotating Bomb Oxidation Test (RBOT-ASTM D2272) conducted under O₂ with initial pressure of 620 kPa and at 150 °C. They proposed the oxidative and thermal degradation mechanism based upon the radical intermediate formation along the alkyl chain attached to the imidazolium cation.^[46] Whereas this study did not probe or confirm the proposed mechanism, others have shown degradation of imidazolium ILs with different alkyl and aryl substituents to take place via a radical formation with advanced oxidation processes including exposure to ultraviolet

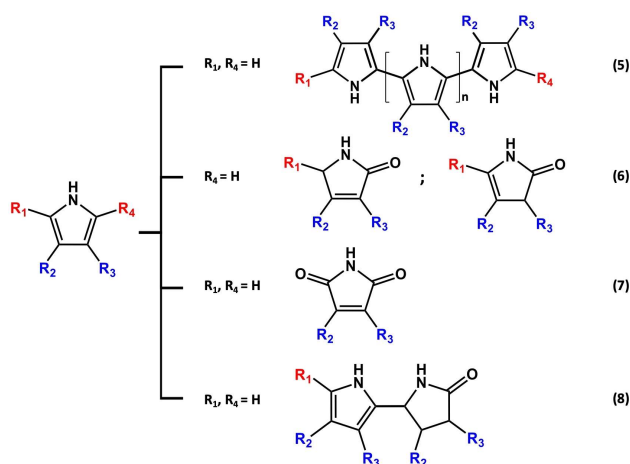
(UV), UV/H₂O₂, UV/TiO₂, 7.2Fe/TiO₂/H₂O₂ systems,^[40,41] as well as excited state oxygen (O₂^{*-} or ¹O₂).^[45,47,48]

Under highly basic conditions (e.g., fuel cells), the degradation of imidazolium-based materials in the presence of an organic solvent or aqueous electrolyte are shown to undergo a nucleophilic attack.^[49–51] The proposed degradation pathways shown in Scheme 1 are reverse Menschutkin (S_N2) reaction (1), nucleophilic addition-elimination followed by ring-opening (2), ylide formation via deprotonation by nucleophile (3), and deprotonation of the ring (4).^[49,52–55] Pathways 1 and 4 involve reactions in the peripheral alkyl substituents, whereas the pathways 2 and 3 are reactions directly involving the imidazolium ring. Density functional theory (DFT) calculations indicate the dominant pathway to be pathway 2 involving the C2 position of the imidazolium ring.^[49] Therefore, bulky substituents at the C2, C4, and C5 positions of the imidazolium are suggested to prevent the deprotonation of liable hydrogen, thus achieving higher stability.^[52,53]

The pairing of the imidazolium cation with a basic anion, such as [2-CNpyr], is desired to increase the absorption capacity at low partial pressures of CO₂. The amine functionality, similar to the case reported for amino-oligomers in the context of their application in DAC can follow basic auto-oxidation scheme.^[56] Although the stabilities of the pyrrolides within ILs have not been examined before, the autoxidation of unsubstituted pyrrole and alkyl and aryl substituted pyrroles under air have been reported.^[57–59] It is agreed that the degradation pathway of pyrrole, under the stimuli of oxidants (e.g., peroxides, singlet oxygen (¹O₂), *meta*-chloroperoxybenzoic acid, ferric chloride), pH, and temperature or by anodic oxidation, often leads to unconstrained de-aromatization, polymerization, and decomposition that form conducting (and/or nonconducting) polypyrrole (5 in Scheme 2).^[57,59–61] Furthermore, depending on the presence and position of the substituting group, products like 3-pyrrolin-2-ones or 4-pyrrolin-2-ones (6) and maleimide (7) are found in addition to dimers (8) through further coupling of pyrrole intermediates (Scheme 2).^[57,59–61] The presence of an electron-withdrawing group on the peripheral substantially decreases



Scheme 1. Degradation pathways of imidazolium cations under nucleophilic attacks in basic conditions.



Scheme 2. Oxidation pathways of pyrroles.

the reaction rate of oxidation, as demonstrated by the photo-degradation of pesticides like Fludioxonil that contain pyrrole.^[62]

Here, the thermal and oxidative stability of [EMIM][2-CNpyr] is studied under air at 50 and 80 °C, thus capturing conditions of a DAC process with absorption-desorption cycles. Under accelerated testing conditions where IL was exposed to pure O₂ and kept isothermally at 80 °C for 7 days, the degradation products and possible mechanisms are determined by NMR, FTIR, MS, and operando GC. The impact of thermal and oxidative degradation of the IL on its density, viscosity, CO₂ absorption capacity, and species diffusivity are examined. Furthermore, MW based regeneration is demonstrated as an alternative approach where no measurable degradation occurred at both 80 and 100 °C. The cyclability of the IL with MW exposure is shown with no CO₂ capacity loss, thus demonstrating the effectiveness of dielectric heating for IL regeneration for DAC for the first time.

Results and Discussion

Analysis of oxidative and thermal degradation

The synthesis of the IL was confirmed by NMR spectroscopy (see the Supporting Information, Figure S1). The accelerated degradation of [EMIM][2-CNpyr] was conducted under the conditions specified in Table 1. Degradation upon extended exposure of the IL to O₂ and heat resulted in thickening and darkening of the liquid (Figure S2, inset). The density (Figure S2) and viscosity (Figure S3) of the degraded samples were measured to be higher than those of the neat IL, suggesting the compacting of the liquid perhaps due to the increased inter- and intramolecular interactions and reactions leading to additional species. Figure 1 shows the product identification by MS of most degraded IL by direct infusion of **Sample 4**.

Both positive and negative MS analysis of the sample is plotted in blue in Figure 1a. The highlighted peaks are the

Table 1. Conditions of the accelerated thermal and oxidative degradation experiments for [EMIM][2-CNpyr].

	Atmosphere	time [days]	Exposure History	
			T [°C]	Method
Sample 1	Air	3	50	Continuous feed of air with 5 sccm flow rate
Sample 2	Air	7	80	Air atmosphere in the head space of 20 mL vial
Sample 3	O ₂	7	80	O ₂ atmosphere in the head space of 20 mL vial
Sample 4	O ₂	7	80	Continuous feed of O ₂ with 5 sccm flow rate

difference between sample infusion (blue) and solvent blank (brown). The parent components [EMIM]⁺ (I) and [2-CNpyr]⁻ (II) appear at $[M]^+ = 111$ and $[M]^- = 91$, respectively. The small satellite peaks at $[M+1]$ for each of these are caused by the presence of the ¹³C isotope (1.11 % of ¹³C natural abundance) in the molecule (percentages listed in Figure 1b). The relative peak heights of the $[M+1]$ peak over the parent peak, can be used to verify the number of carbon atoms within the molecules. The ratio of 6.58 % for a six-carbon molecule and 5.53 % for a five-carbon molecule are expected (Detailed calculation given in Supporting Information). Indeed, these values are close to that of 6.46 % of (I) and 5.17 % of (II) as calculated from the observed intensity ratios in Figure 1b.

Based on the MS analysis, there are two oxidative degradation products labeled as (III) and (IV) in Figure 1b representing the oxidized cation and the oxidized anion, respectively.^[62] Although there is no reporting directly on the oxidation of imidazolium under O₂ at 80 °C, the most relevant studies that involve the presence of [OH]⁻, ¹O₂, and [O₂]⁻ point to the most reactive site being the C2 position on the imidazolium compounds.^[47,49,63] Therefore, a similar nucleophilic attack by oxygen radical on the cation likely takes place at the C2 position (Scheme 3a), whereas radical formation in the anion is most likely at the α position (Scheme 3b), owing to the greater number of intermediate resonance states in contrast to the β or γ carbon (Scheme 3b). The oxidative degradation of the cation begins with the radical cleavage of hydrogen on the C2 carbon, as shown in Scheme 3a, followed by the attack of an oxygen molecule that results in the formation of a peroxide radical. With the capture of a hydrogen radical, the peroxide radical then turns into peroxide, which breaks down and eventually produces the oxidized cation. The oxidized cation is believed to be in equilibrium with its amide tautomer. The oxidation of the anion is expected to follow a similar pathway as shown in Scheme 3b. It is noteworthy that both oxidative degradation products were observed even under mild degradation environments of **Sample 1** (Figure S4).

Along with the oxidative products determined in **Sample 4**, we identified an additional peak at $m/z = 181$ in the negative scan (Figure 1a), representing the anion dimer that was not observed in **Sample 1**. We speculate this dimerization to be dependent on the radical concentration for the anion, which increases with greater oxygen exposure at elevated temper-

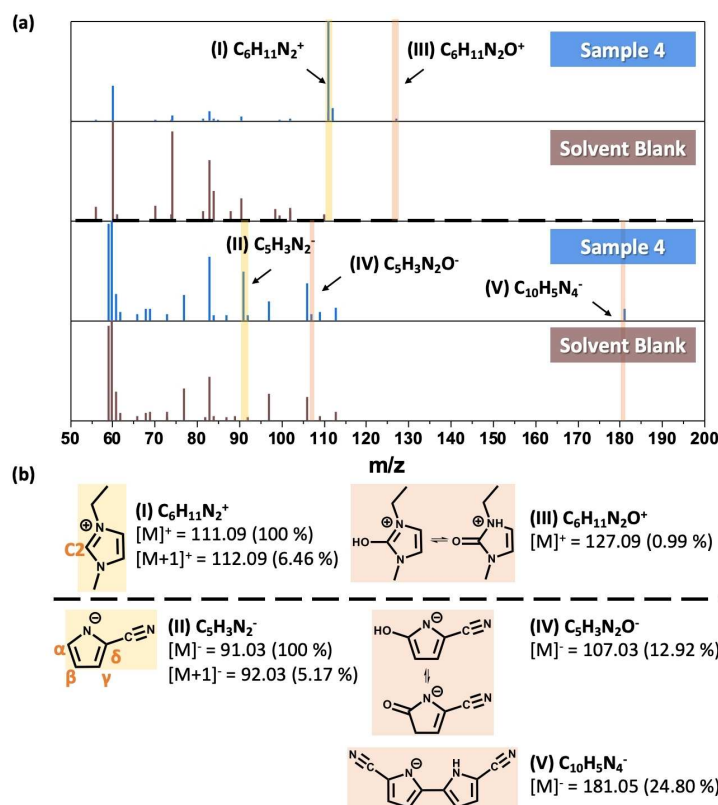


Figure 1. (a) ESI-MS for **Sample 4**. The top two scans are the positive scans and the bottom two are the negative scans. Solvent blank (brown); sample (blue). Note that some of the impurities from the solvent also appear in the sample spectra due to pre-contamination of the ESI-MS chamber. The peaks highlighted in yellow are the cation and anion of [EMIM][2-CNpyr]. The spectra for **Sample 1** are shown in Figure S4. (b) Molecular structure of EMIM⁺ and 2-CNpyr⁻ of the IL (in yellow) and the degradation components (in orange) detected by ESI-MS: cation (I); anion (II); oxidized cation (III); oxidized anion (IV); anion dimer (V). The peak intensities in the negative scans were normalized by that of 2-CNpyr⁻.

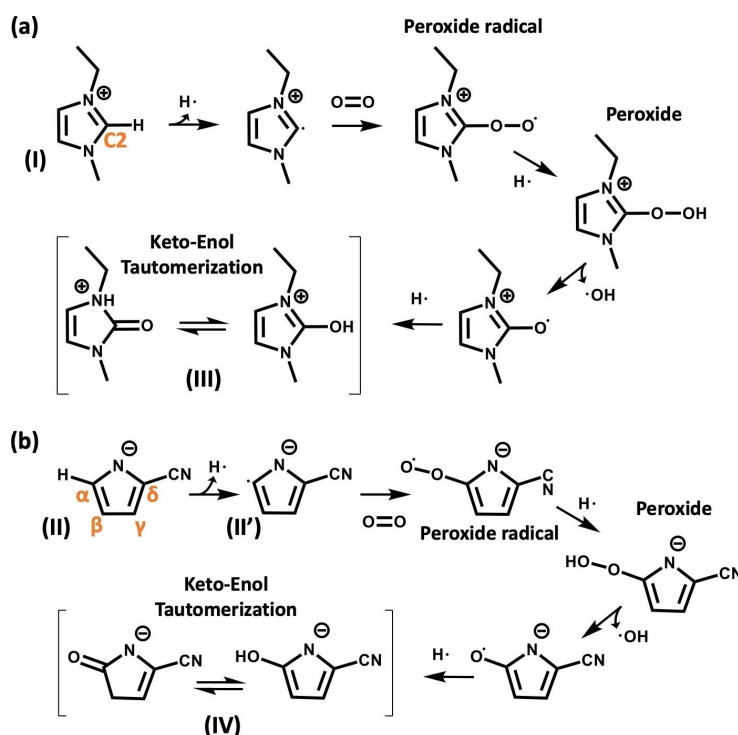
atures (Scheme 4a). The anion dimer forms through the C–C bond formation of the carbon radical at the α position of the anion and the hydrogen radical results in H₂ gas. The anion dimer is likely to be a dianion [C₁₀H₄N₄]²⁻ but could be readily protonated to be [C₁₀H₅N₄]⁻. Different from the formation of ring-like oligomers or linear polymers from pyrrole under various stimuli,^[57,60,64–67] the lack of liable proton at the δ carbon limits the chance of chain propagation and ends the decomposition of the anion with a dimer. These results are in agreement with the report by Li et al. on the radical-induced degradation of amino-oligomer sorbents where varying oxidative stability (and kinetics) was observed based on the local environment of the amine.^[56]

To confirm the proposed degradation reactions, a series of analysis consisting of GC (for gaseous side products), NMR, and FTIR was performed. Off-gas operando GC analysis was conducted on **Samples 1** and **4** throughout the period of the accelerated degradation experiments. H₂ evolution from **Sample 4** was detected by TCD2 (Figure 2a); it was quantifiable after 6 h (Figure 2b).

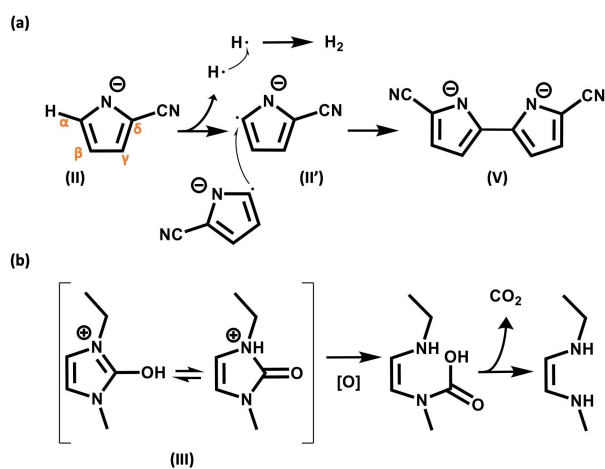
We interpreted the H₂ to be coming from the cleaved-off hydrogen radical from the α position (Scheme 4a), leading to the formation of the anion dimer observed in MS. The dimerization in **Sample 4** is further supported by ¹³C NMR in

Figure 3 (small peaks highlighted in orange). In contrast, neither H₂ evolution nor the anion dimerization were observed in other degraded IL samples. A possible explanation for this observation is the stronger dependence of these side reactions to O₂ concentration, in which case the likelihood of two anion radicals being near each other is high enough to form the dimer.

The regions highlighted in green in Figure 4 confirm the formation of the proposed oxidized products (hydroxide O–H stretching at 3300 cm⁻¹) and their amide tautomers (amide N–H bending at 1560 cm⁻¹ and amide C=O stretching at 1680 cm⁻¹), as well as the ring-opening product (secondary amine N–H stretching at 3330 cm⁻¹, alkenyl C–H stretching at 3090 cm⁻¹, and alkenyl C=C stretching at 1620 cm⁻¹). The orange region suggests the potential oxidation of cyano groups under extensive oxidative condition in **Sample 4**. It is also possible that additional –CN vibration is due to the presence of the different environments with the anion dimer formation. These observations in NMR and FTIR strengthen our proposed anion dimerization and ring-opening reaction pathways in Scheme 4. Aside from the dimerization reaction of the anion, we also observed the emission of CO₂ gas starting from day 6 in the chromatogram of TCD2 (Figure 2a), which is highlighted in the gray shaded region in Figure 2b. We hypothesize that the emission of CO₂ is from the pathway shown in Scheme 4b,



Scheme 3. Proposed oxidative pathway of (a) EMIM⁺ and (b) 2-CNpyr⁻ taking place under air at 50 °C (**Sample 1**) and pure O₂ atmosphere at 80 °C (**Sample 4**) in the accelerated degradation tests.



Scheme 4. (a) Dimerization and H₂ evolution from the anion radical (II'). (b) CO₂ evolution from the ring-opening mechanism of cation-derived keto tautomer (III).

where a ring-opening reaction of the keto tautomer of the oxidized cation takes place. Based on these results, we conclude that the oxidative degradation reactions strongly depend on the temperature and O₂ concentration.

The degradation-derived CO₂ binds back to the IL as indicated by the gray highlighted peaks in ¹³C NMR (Figure 3) and FTIR (Figure 4) that correspond to the bound CO₂. The split of the cation peaks (g' and i') and the shift of the anion peaks (d', e', f', h', and j') in NMR present consistent behavior with our

previous study, where the specific CO₂ binding mechanism with this IL was reported.^[37] Figure 3b shows the CO₂ complexed cation and anion species of carboxylate and carbamate, respectively, in the middle. We considered the possibility of potential oxidation of polyethylene tube in the gas line as the CO₂ source; however, experiments carried out without these tubing components (**Samples 2** and **3**) yielded similar results of CO₂ evolution and binding to IL. Therefore, we conclude the evolution of CO₂ to be a product of the cation degradation as suggested in Scheme 4b.

As the exact molecular structures of some degradation products were difficult to fully characterize by FTIR, NMR or MS, owing to their low concentrations, potential degradation pathways are proposed based on cross-referencing the spectroscopic results (Figure 5). The viscosity increase in degraded IL may be related to the formation of stronger Coulombic interactions between the cation and the dianion, as well as H-bonding between the alcohol and amine groups, in addition to the oxidized and polymerized products.

The impact of anion nucleophilicity on stability

The nucleophilicity of the anion was reported to be a critical factor for stability.^[68] A ramped gravimetric analysis of [EMIM]-based ILs (or salts) with varied anion nucleophilicity (Table 2) was performed with TGA.

ILs with low-nucleophilicity anions, such as [TFSI] and [TCM], were observed to have the highest thermal stability of at least

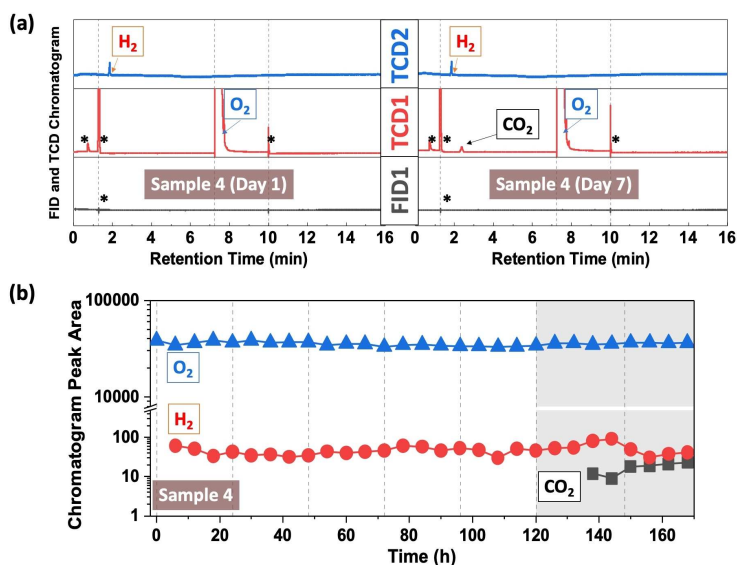


Figure 2. (a) Gas chromatograms of the off-gas from the degrading experiments of **Sample 4** at day 1 (left panel) and day 7 (right panel). FID1 shows no volatile organics. TCD1 (mobile phase: He) shows CO_2 peak after long exposure to O_2 . TCD2 (mobile phase: N_2) shows H_2 peak. The artificial peaks (labeled with asterisks) originate from the pressure deviation within the GC column due to pneumatically controlled valve events. (b) Gas chromatography of the off-gas from **Sample 4** with data collected in 6 h intervals from all three detectors. The presence of CO_2 peak (black squares) was highlighted with grey background.

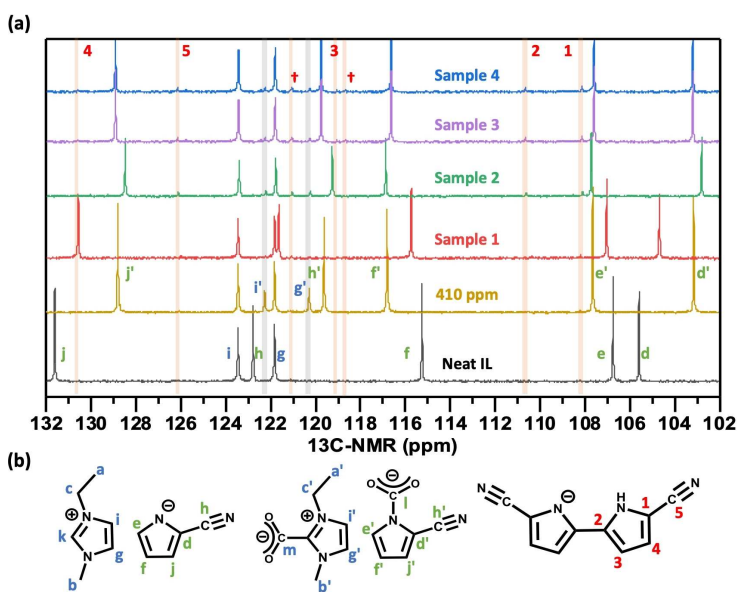


Figure 3. (a) ^{13}C NMR spectra of the fresh IL and the degraded IL samples showing only 102–132 ppm region. The cation splitting and shifting for CO_2 binding is highlighted in grey and the anion dimer is highlighted in orange. The spectra of CO_2 -absorbed IL from the absorption experiments under 410 ppm CO_2 (in khaki color) we reported previously^[29] is included as a point of reference. The symbol “+” marks the peaks of an unidentifiable decomposed component that has very low concentration. The full ^{13}C NMR spectra are given in Figure S5. (b) Labeling of the NMR peaks. The protons on IL are labeled with (a, b, c, ...), the CO_2 bound products with (a', b', c'...), and the anion dimer with (1, 2, 3, ...).

350 °C (Figure 6a), which is even better than the cation precursor [EMIM][I]. This demonstrates that the thermal decomposition of [EMIM]⁺ cannot be decoupled from its counterion, and, in fact, the anion has a dominant role in driving the degradation of the IL. The first derivative of TGA curve (mass loss) against temperature clearly demonstrates the trend (Figure 6b). The increase in the nucleophilicity of the anion from

[TFSI] to [2-CNpyr] lowers the decomposition temperature by 100 °C. When the electron withdrawing cyano ($\text{C}\equiv\text{N}$) substitution is eliminated as in the case of [Pyr], thus increasing the nucleophilicity of anion, the resulting compound [EMIM][Pyr] demonstrates very low thermal stability. The strong nucleophilic [Pyr] decomposes the cation. In fact, the decomposition is so profound that [EMIM][Pyr] is not even stable as evident from

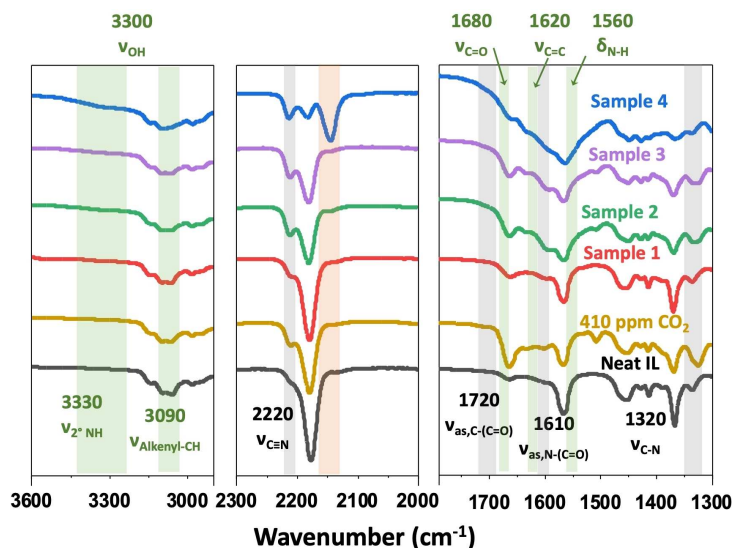


Figure 4. FTIR spectra of the fresh IL and degraded IL (**Samples 1–4**). Regions highlighted in grey are the absorption peak shifts due to CO₂ binding. Region highlighted in orange indicates the strong C≡N stretch of the oxidized cyano group and possibly the anion dimer. Regions highlighted in green are potential formation of secondary amines (3330 cm⁻¹), hydroxy (3300 cm⁻¹), and alkenyl groups (3090 cm⁻¹ and 1620 cm⁻¹), that are not detected with the previously discussed methods, however their presence support the proposed mechanism of CO₂ evolution. The full FTIR spectra are given in Figure S6.

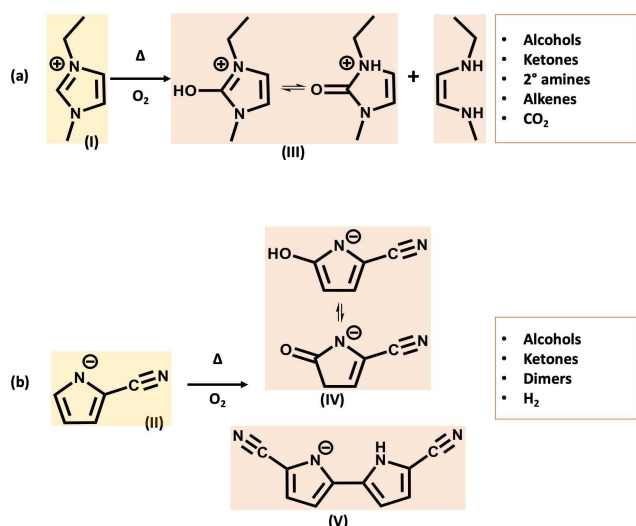


Figure 5. Proposed mechanism of oxidative and thermal decomposition of [EMIM][2-CNpyr] under continued exposure to O₂ and heat (80 °C for 7 days). The oxidation-derived compounds of EMIM⁺ and 2-CNpyr⁻ further produce CO₂ and H₂, as detected by GC.

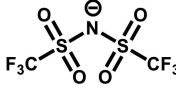
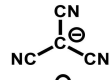
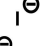
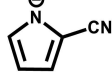
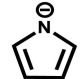
¹H NMR (Figure S7), where it readily degrades. Under air, the thermal stability of [EMIM][2-CNpyr] (dashed line in Figure 6) was also found to be lower when compared to N₂ environment (solid line) by about 10 °C in decomposition temperature.

Impact of temperature and oxygen on ion diffusivities and CO₂ capacity

The self-diffusivity (*D*) of the cation and anion were measured by ¹H DOSY NMR (see Experimental Section and Figure 7a). An

example of the ¹H pulse field gradient (PFG) NMR for diffusivity calculation is shown in Figure S8. We would like to point out the limit of ¹H NMR (and ¹H DOSY NMR), in which [EMIM]⁺ and [EMIM]⁺-derived components cannot be resolved effectively as separate entities; however, they appear as a single peak due to the low concentration of the [EMIM]⁺-derived components and the interactions among them via H-bonding. A similar limitation also applies to [2-CNpyr]⁻. Although both the [EMIM]⁺ and [2-CNpyr]⁻ ions are composed of five-member heterocyclic aromatic ring-structure with short pendent groups, giving similar hydrodynamic radius, the diffusivity of anion (*D*⁻) in the neat IL is observed to be slightly slower than that of cation (*D*⁺). This is likely due to the stronger H-bonding interactions between the conjugated [2-CNpyr]⁻/2-CNpyrH adduct.^[17,37] The *D*⁺/*D*⁻ ratio is denoted as the “*R* value,” which represents a measure of change in the surrounding solvation environment. The *R* value of **Sample 1** (1.18) is similar to that of neat IL (1.21), whereas **Sample 4** gives an *R* value of 1.02 and a diffusivity that is one order of magnitude lower than other samples. This suggests a very different chemical environment in **Sample 4**, where the ions are relatively confined by higher order interactions in the presence of intermolecular H-bonds that thicken and compact the liquid, in alignment with the higher viscosity measured, as opposed to **Sample 1** and the neat IL.

Figure 7b shows the CO₂ capacity of the neat and the degraded IL **Samples 1** and **4**. The capacity was calculated by quantitative ¹³C NMR by the integration of carbamate (CO₂-anion complex; 146 ppm), carboxylate (CO₂-cation complex; 154 ppm), and bicarbonate (CO₂-water; 158 ppm). With mild exposure history in **Sample 1**, we observed similar CO₂ capacity under 410 and 2500 ppm of CO₂ in N₂ post decomposition tests. However, the measured capacity of **Sample 4** decreased by about 50%, which could be traced back to the loss of both

Anion	Full name	Molecular structure	Donor number [kcal mol ⁻¹] ^[9,69]
[TFSI]	bis(trifluoromethanesulfonyl) imide		11.2
[TCM]	tricyanomethanide		26.1
[I]	iodide		59.3 ^[a]
[2-CNpyr]	2-cyanopyrrolide		N/A
[Pyr]	pyrrolide		N/A

[a] Donor number measured with 1-octyl-3-methylimidazolium iodide [OMIM][I], instead of [EMIM][I].

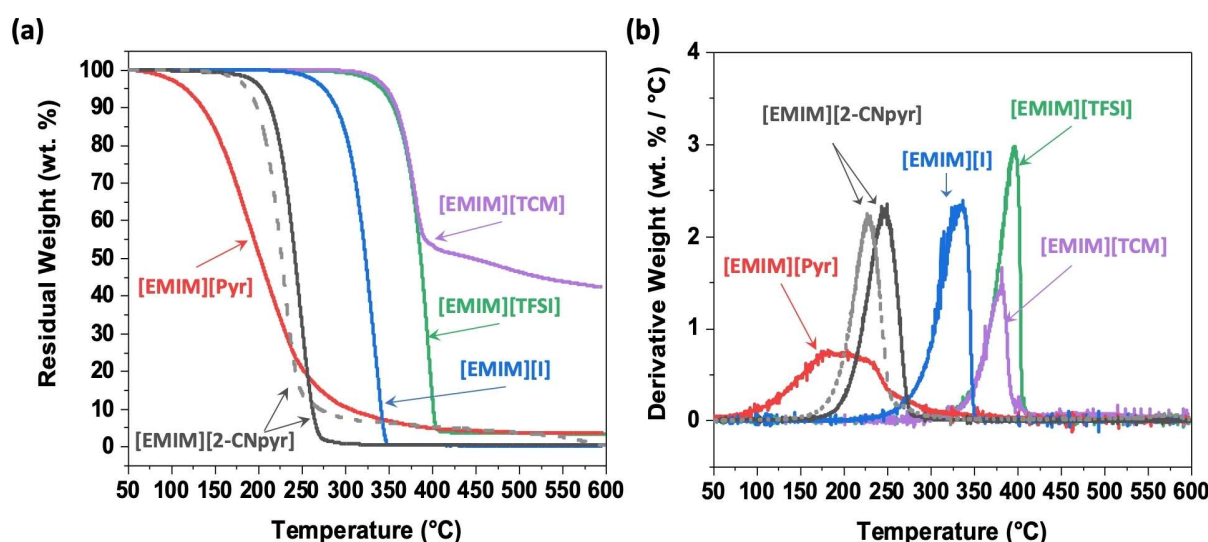


Figure 6. (a) TGA of samples in Table 2 with heating to 600 °C under N₂ at 10 °C min⁻¹. (b) The first derivative of TGA weight loss against the heating temperature. The thermogram plotted as a dashed line represents the decomposition of [EMIM][2-CNpyr] under air, where a slightly different degradation pattern is observed, notably the higher char yield.

active sites of carboxylate on cation (154 ppm) and carbamate on anion (146 ppm). We hypothesized the deactivation of CO₂ binding sites to be related to the degradation of the IL itself, and possible hindrance from the intramolecular H-bond, which may impede CO₂ from accessing the active sites.

Stability against MW exposure and CO₂ release by dielectric heating

Microwave-assisted desorption was performed at a constant temperature (80 and 100 °C in two consecutive cycles) by auto-adjusting the microwave power (0–10 W at 2.45 GHz), following CO₂ absorption at 25 °C (Figure 8). The setup is shown schematically in Figure S9 and the representative temperature and MW power profile during desorption are shown in Figure S10.

Absorption was performed by contacting the IL with a feed gas of 5000 ppm CO₂ in synthetic air (80:20 N₂/O₂) at 25 °C with 0% RH. To achieve 50% RH ($P_{\text{H}_2\text{O}} = 15.9$ mbar), the feed gas was bubbled through a water reservoir. Desorption was performed by dielectric heating at 100 °C in the first cycle and 80 °C in the second cycle under dry N₂. When the absorption was under 0% RH, both the absorbed and desorbed amounts of CO₂ are the same in both the 1st and 2nd cycles (Figure 8top), thus demonstrating effective desorption and cyclability. Here, the absorption time was limited to 2.5 h and the absorbed CO₂ does not reflect the thermodynamic equilibrium at 25 °C due to slow absorption rate. The rate of desorption is about 7.5 times greater than the absorption rate (Figure 8bottom), likely resulting from reduced viscosity at higher temperatures and direct molecular level heating. In fact, desorption is rapid, and

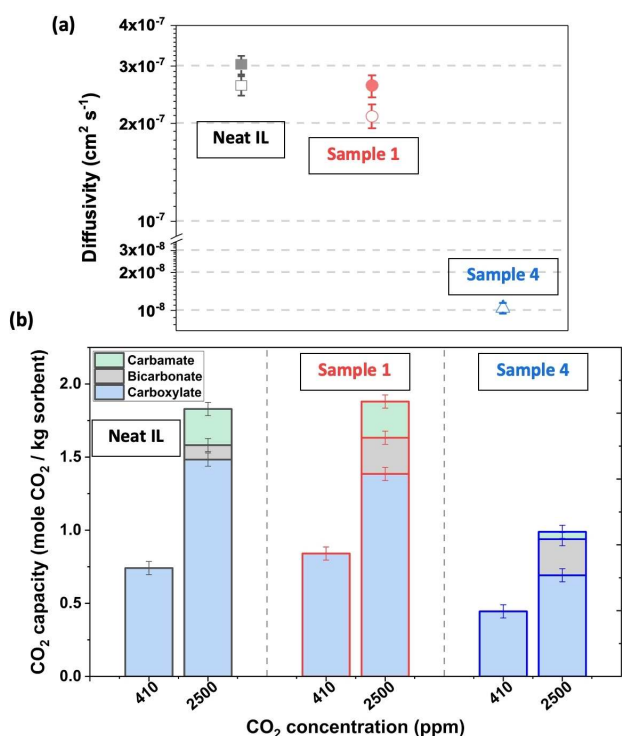


Figure 7. (a) Self-diffusivity of cation (filled symbols) and anion (open symbols) of [EMIM][2-CNpyr] measured by ^1H DOSY NMR. The D^+ and D^- values of Sample 4 closely overlap one another. (b) Breakdown of CO_2 capacity based on the quantified ^{13}C NMR peaks of carbamate (CO_2 -anion complex), carboxylate (CO_2 -cation complex), and bicarbonate (CO_2 -water) for the fresh IL (black outlined bars), Sample 1 (red outlined bars), and Sample 4 (blue outlined bars). The uncertainty of the breakdown capacity is calculated from the signal to noise ratio to be less than 0.05 mol CO_2 per kg of sorbent.

half of the absorbed CO_2 is released within the first three minutes.

With absorption at 50% RH, working capacity (difference between absorbed and desorbed CO_2 in a cycle) is decreased despite the fact that the absorbed amount of CO_2 is slightly increased. Therefore, the regeneration efficiency is around 80% (Figure 8right). The increased absorption capacity under humid feed conditions is likely due to the CO_2 uptake by the absorbed water in the IL as it is known that water reacts with CO_2 in basic conditions forming bicarbonate and carbonate.^[37] However, it is also known the reaction enthalpy of bicarbonate and carbonate formations are higher than that of carboxylate and carbamate that forms from CO_2 absorption by the IL.^[29,37,70] Therefore, it is not surprising that the regeneration efficiency is lower in the 2nd cycle where the temperature is lower. The IL darkened in color after dielectric heating at 100 °C for 1 h, owing to initiated IL oxidation, which is probably very low in amount and thus could not be detected.

After a total MW cycle of 6 h (4 h of pretreatment at 50 °C, 1 h of 1st desorption at 100 °C, and 1 h of 2nd desorption at 80 °C), the stability of IL (treated under 0% RH) was confirmed by NMR (Figure S11) and FTIR (Figure S12) spectroscopy. Viscosity of the MW regenerated IL after the completion of breakthrough measurements under 0% RH was measured as

85 cP at 25 °C, which is lower than the measured value of 90 cP for aged IL at 50 °C after 3 days by conventional heating, in comparison to 70 cP for the fresh sample prior to any absorption-desorption history.

To compare MW regeneration with the convectional heating, parallel experiments were performed up to 8 absorption-desorption cycles (16 h total). Cycling was performed with a dry feed gas of 5000 ppm CO_2 in synthetic air for 60 min at 25 °C, followed by desorption under N_2 for 45 min at 80 °C in both experiments using the same setup. The only difference was that the convectional heating was performed by immersing the sample chamber in a pre-heated oil bath at 80 °C as the heat source instead of dielectric heating by MW. As shown in Figure 9, the MW regeneration resulted in similar working capacities to convectional heating but led to slightly more efficient and stable regeneration efficiency. Following cycling, both samples were characterized by NMR to identify possible degradation products. However, none was observed (Figure S14). These results demonstrate the utility of MW as a viable alternative to conventional heating in IL regeneration in CO_2 capture processes.

It is shown here that the CO_2 -reactive IL is susceptible to dielectric heating and the desorption can be achieved effectively considering the high viscosity of the IL that limits mass transport. Although [EMIM][2-CNpyr] was found to undergo thermal and oxidative degradation under O_2 at 80 °C for 7 days, therefore losing 50% of its CO_2 capacity, it is relatively stable upon cycling under air feed gas and 80 °C regeneration. These results further demonstrate the superior stability of the functionalized IL, compared to the solid amines where CO_2 capacity loss in the orders of 80% and 61% have been reported under dry air at 120 °C^[71] and 80 °C^[72] for 7 days, respectively.

Conclusions

The CO_2 -reactive IL [EMIM][2-CNpyr] was exposed to air and O_2 at 50 and 80 °C for durations of 3 and 7 days to examine the possible oxidative thermal degradation reactions that could occur under a repetitive thermal-swing process that a sorbent undergoes in CO_2 capture. The results from a series of analytical measurements suggest oxidation of both ions and ring opening of the imidazolium by radical and $\text{S}_{\text{N}}2$ reaction mechanisms, respectively. These reactions were encouraged by the nucleophilicity of the anion producing mostly pyrrole dimer, ketones, and alkenes in addition to H_2 and CO_2 gases. Although the CO_2 reactivity of the IL sorbents relies on nucleophilic functional groups, stronger nucleophilicity negatively impacts sorbent stability upon long-term exposure to thermal cycling, as evidenced by the measured increase in viscosity and loss of CO_2 capacity. Therefore, balancing of the nucleophilicity of an IL sorbent for CO_2 capacity and regeneration temperature is important. To eliminate long exposures to high temperatures under conventional heating, MW regeneration was demonstrated as an alternative where no measurable degradation products were found after a total of 6 h exposure to MW at 50–100 °C. Although this study demonstrates the susceptibility of IL

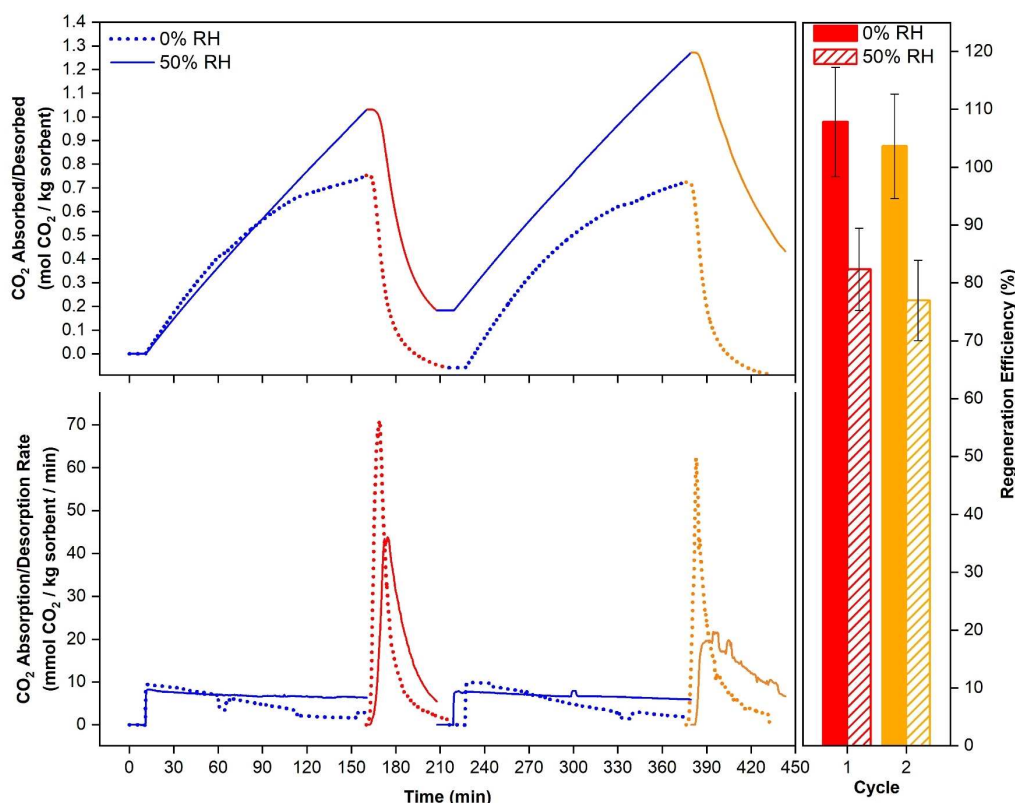


Figure 8. CO₂ breakthrough curves (top left), CO₂ absorption/desorption rate (bottom left), and regeneration efficiency (right) for [EMIM][2-CNpyr] for two consecutive cycles. Blue lines represent absorption at 25 °C with both 0% RH (dotted lines) and 50% RH (solid lines) feed gas (5000 ppm CO₂ in 80:20 N₂/O₂). Red lines represent MW-based desorption at 100 °C in 1st cycle and 80 °C (orange) in 2nd cycle. Regeneration efficiency is defined as the ratio of the amount of CO₂ desorbed per CO₂ absorbed. Sample was pretreated by dielectric heating at 50 °C for 4 h. The microwave (2.45 GHz) power was automatically controlled between 1–10 W for the set desorption temperatures; power and temperature profiles for the 2nd cycle (0% RH) are shown in Figure S10 as an example.

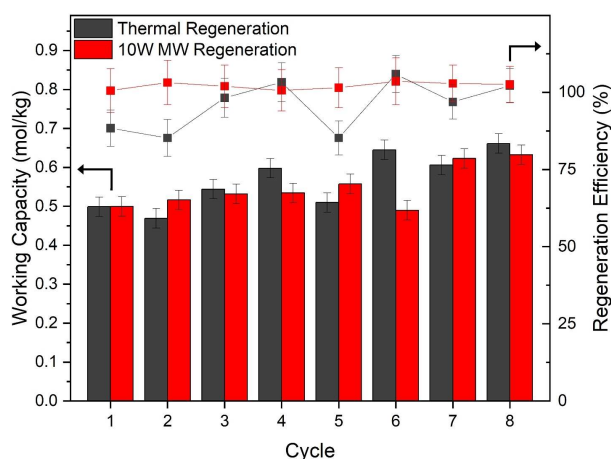


Figure 9. Working capacity (bars) of [EMIM][2-CNpyr] during 8 cycles (16 h total) of absorption (25 °C) under 5000 ppm CO₂ and desorption at 80 °C under N₂, comparing the convective heating (gray) and dielectric heating by MW (red) for regeneration. The regeneration efficiency (squares) is calculated by dividing the amount of CO₂ released by the amount of CO₂ absorbed during a given cycle.

for MW based regeneration and desorption of CO₂, it should be further investigated whether there is structure-induced release of CO₂ besides the dielectric heating effects.

Experimental Section

Materials

The IL precursor, 1-ethyl-3-methylimidazolium iodide ([EMIM][I], > 98%) was purchased from TCI America. Reagent grade solvents of methanol, acetone, isopropanol, anion precursor pyrrole-2-carbonitrile (97%), and anion exchange resin (AER) Amberlite® IRN-78 (hydroxide form) was purchased from Alfa Aesar (Thermo Scientific). Anion exchange resin was rinsed with methanol at least three times and vacuum dried under ambient temperature before use. Paramagnetic compound chromium (III) acetylacetonate (Cr(acac)₃) and pyrrole (98%) were purchased from Sigma-Aldrich (Millipore Sigma). The deuterated solvent DMSO-d₆ (10 mL, 99.9%) was purchased from Cambridge Isotope Laboratories. The non-nucleophilic (also non-CO₂ reactive) ILs 1-ethyl-3-methyl-imidazolium bis(trifluoromethanesulfonyl)imide ([EMIM][TFSI], 99%) and 1-ethyl-3-methyl-imidazolium tricyanomethanide ([EMIM][TCM], 99%) were purchased from Iolitec Inc, Germany. The thrift-grade NMR tubes (5 mm diameter; 7" length) and coded closed caps were purchased from Wilmad Labglass. The NMR coaxial tube sets (NE-5-CIC and NE-UP5-7) were purchased from New Era Enterprises, Inc. Gas tanks of nitrogen (N₂; Ultra High Purity (UHP), argon (Ar; UHP), helium (He; UHP), carbon dioxide (CO₂; bone dry), oxygen (O₂; UHP), hydrogen (H₂; UHP), and synthetic air (Air; N₂ 80% and O₂ 20%) were purchased from Airgas, Cleveland.

Synthesis

The synthesis of [EMIM][2-CNpyr] and [EMIM][Pyr] started with gradual anion exchange of precursor (10 g [EMIM][I] in 100 mL methanol) from I⁻ to OH⁻ at ambient temperature of 22 °C. The use of AER was monitored to be 5 g per mmol of [EMIM][I]. The absence of residual iodide in the [EMIM][OH] intermediate was confirmed by (0.171 N) silver nitrate test where no visible white or yellowish silver(I) iodide precipitate was observed. Anion precursor was then added dropwise to the [EMIM][OH]/methanol intermediate solution ([EMIM][OH]: anion precursor 1:1.05 mole ratio) and agitated at 22 °C overnight. The resulting solution was then transferred to a round bottom flask where excess solvent was removed by a rotary evaporator with a vacuum pump (Edwards E2M0.7) at 50 °C. The removal of residual moisture was carried out in a switch valve-controlled steel chamber under high vacuum of < 100 mTorr with an Edwards RV-8 pump at 70 °C overnight. The molecular structure of [EMIM][2-CNpyr] was confirmed by ¹H NMR and the peak assignment confirmed by heteronuclear single quantum coherence (HSQC), as shown in Figure S1. Combustion ion chromatography (Atlantic Labs) confirmed the halogen content in [EMIM][2-CNpyr] to be lower than its detection limit (0.25%). Elemental analysis calculated for C₁₁H₁₄N₄: C 65.32, H 6.98, N 27.70; found: C 62.78, H 7.15, N 26.87.

Characterization methods

The molecular structure of ILs were characterized by nuclear magnetic resonance spectroscopy (NMR: ¹H, ²H, and ¹³C NMR on a Bruker Avance III HD 500 MHz NMR Spectrometer equipped with Broadband Prodigy TCI CryoProbe). Fourier-transformed infrared spectroscopy (FTIR) was taken on a Nicolet iS50 (Thermo Scientific) with built-in mid- and far-IR capable diamond attenuated total reflection. The water contents of the IL samples were measured by Karl Fisher titration (Metrohm Coulometric; KF 889D) to be all less than 1000 ppm. Densities were measured with a vibrating U-tube density meter (Anton Paar; DMA 4500 M) within its own temperate control chamber (±0.03 K). The uncertainty of density is ± 0.00005 g cm⁻³. Viscosity was measured with a microchannel viscometer (Rheosense; MicroVISC) in temperature control unit (± 0.10 K). The uncertainty of viscosity is about 2%. Thermal stabilities were measured by a thermogravimetric analyzer (TGA, Q500) with a few drops (ca. 15 μg) of anhydrous IL sample in a platinum pan. The samples were tested with a temperature sweep from 50 to 600 °C at a rate of 10 °C min⁻¹, under either N₂ or air atmosphere.

Accelerated degradation tests and component analysis

2 mL of IL sample was placed in a 20 mL glass vial and agitated at 60 rpm with a magnetic stirrer (IKA C-MAG HS 7 digital). The head space within the glass vial was about 18 mL. A total of four accelerated degradation tests were performed, corresponding to **Samples 1–4** (Table 1). **Sample 1** and **Sample 4** were continuously contacted with air and O₂, respectively, and the evolving components were sent to the GC for analysis. Evolving gas analysis was carried out by a customized GC (Agilent GC 7890B) equipped with two thermal conductivity detectors (TCD1, mobile phase: He; TCD2, mobile phase: N₂) and one flame ionization detector (FID1; mobile phase: He). Degradation tests for **Sample 2** and **3** were performed in gas-tight 20 mL glass vials, with about 18 mL of air and O₂ as the atmosphere, respectively. The targeted atmosphere was purged into the vial for 10 min to replace the atmosphere before sealing the vial with lid and parafilm. Samples were degassed overnight by pulling vacuum and kept in an argon filled glovebox (VTI, with H₂O and O₂ both less than 0.1 ppm). The water content before and after the degradation tests were measured by KF titration to be

< 1000 ppm. **Samples 1** and **4** were analyzed by electrospray ionization mass spectroscopy (ESI-MS; TSQ Quantum XLS Ultra). IL samples with a concentration of 25 mM in acetonitrile/water (50:50 v/v) mixture were directly infused and scanned in the range of *m/z* 50–600, with 0.1 mol% of acetic acid as additive for the positive scan and with no additive for the negative scan.

CO₂ capacity measurements before and after degradation

CO₂ capacities were measured for the neat IL and **Samples 1** and **4** following a similar procedure as described previously.^[37] Briefly, mass flow controllers (MFC; Brooks 5850i) were used to create mixed anhydrous feeds of CO₂ and N₂ at 410 ppm and 2500 ppm of CO₂. Complete mixing of the gas was ensured in a 300 mL metal chamber (Swagelok) within an isothermal incubator (HettCube 400R; Across International LLC) at 22 °C prior to the absorption cell (20 mL glass vial). The CO₂/N₂ gas flow rate and composition were confirmed by an ADM 2000 Flowmeter (J&W Scientific Inc., acquired by Agilent) and an infrared gas analyzer (SBA-5, PPSystems Inc.), respectively. Analysis of the absorbed CO₂ in the IL was done by quantitative ¹³C NMR, following a previous report.^[37]

Ion self-diffusivity measurements

Diffusion coefficient of the ions within the IL samples (**1** and **4**) was measured by Diffusion-Ordered Spectroscopy (DOSY) NMR using a bipolar gradient (ledbpgp2 s) pulse sequence on a Bruker 500 MHz NMR (¹H Larmor frequency of 500 MHz) with Z-gradient diffusion probe. The signal was accumulated over 16 transients with 4 s delay at 298 K. The isotopic self-diffusivity (*D*) of ions was calculated by using Equation (1).

$$M(g) = M_0 e^{[-(\gamma g \delta)^2 D (\Delta - \frac{\delta}{2})]} \quad (1)$$

where γ is the gyromagnetic ratio, g is the magnitude of the gradient pulse, δ is the duration of the gradient pulse, and Δ is the interval (drifting time) between two gradient pulses in opposite directions. M_0 is the strength of magnetization without pulse field gradient applied, whereas $M(g)$ is a function of the applied pulse field gradient. Δ and δ were set to be 190 ms and 3 ms, respectively.

CO₂ absorption and MW-assisted CO₂ regeneration

For CO₂ breakthrough measurements, 5 mL of IL sample was placed in a 125 mL flat-bottom Pyrex glass flask and the sample was pretreated by microwave exposure at 50 °C for 4 h under air flow to confirm stability. Following this, absorption measurement was performed by contacting the sample with anhydrous CO₂/N₂/O₂ gas feed (5000 ppm CO₂ in synthetic air; 80:20 N₂/O₂) at a flow rate of 400 mL min⁻¹ for 2.5 h while constantly stirring the liquid. Absorption was followed by desorption through microwave exposure for 1 h. The setup is shown in Figure S9 and a representative power and temperature profile are shown in Figure S10. The amount of CO₂ absorbed/desorbed was determined by quantitative ¹³C NMR analysis of the liquid and the CO₂ in the exhaust was quantified by the IR analyzer according to the procedure reported previously.^[38] Dielectric heating to maintain a constant temperature of the liquid sample for desorption at 80 or 100 °C (IR temperature sensor with uncertainty of ±1 °C) was achieved by automatically adjusting the continuous MW power (CEM Discover 2.0; 2.45 GHz, 1–300 W). The desorbed CO₂ was swept by N₂ flow (400 mL min⁻¹) to the IR gas sensor. This procedure was repeated for the second absorption-desorption cycle. Possible degradation during MW exposure was

assessed by NMR and FTIR spectroscopy. The viscosity of the sample post cycling was also measured as described earlier.

Author Contribution Statement

Y.-Y. L. performed accelerated degradation tests, thermal stability tests, ¹H-DOSY NMR measurements, and quantitative ¹³C NMR. E. C. synthesized ILS, proposed degradation mechanisms, and analyzed post MW spectroscopy measurements. A. K. designed the MW-assisted breakthrough setup and performed cyclability experiments. Y. P. performed the FTIR and GC-MS measurements. R. D. assisted in synthesis, NMR, and MW regeneration experiments. M. K. K. oversaw the GC-MS and FTIR measurement and analysis. B. G. developed the idea, designed the experimental plan, and oversaw the analysis. All of the authors contributed to writing the manuscript.

Notice of Copyright

This manuscript has been authored by UT-Battelle, LLC, under contract DE-AC05-00OR22725 with the US Department of Energy (DOE). The US government retains and the publisher, by accepting the article for publication, acknowledges that the US government retains a nonexclusive, paid-up, irrevocable, worldwide license to publish or reproduce the published form of this manuscript, or allow others to do so, for US government purposes. DOE will provide public access to these results of federally sponsored research in accordance with the DOE Public Access Plan (<http://energy.gov/downloads/doe-public-access-plan>).

Acknowledgements

This study was supported by the U.S. Department of Energy, Office of Science, Basic Energy Science under award number DE-SC0022214 (the GC-MS studies for oxidative degradation and microwave-assisted breakthrough measurements) and an Early Career Faculty grant from NASA's Space Technology Research Grants Program under Award No. 80NSSC18K1505 (synthesis, thermal degradation, and spectral characterization). The authors acknowledge the Case Center for Proteomics and Bioinformatics at CWRU for access to mass spectroscopy and Soft Matter Characterization Laboratory for the access to TGA. Authors thank Dr. Nalinda Wickramasinghe at the Northeast Ohio High Field NMR Consortium at CWRU for his assistance with DOSY measurements.

Conflict of Interests

The authors declare no conflict of interest.

Data Availability Statement

The data that support the findings of this study are available in the supplementary material of this article.

Keywords: carbon capture · dielectric heating · electromagnetic wave · oxidative degradation · thermal degradation

- [1] J. F. Brennecke, E. J. Maginn, *AIChE J.* **2001**, *47*, 2384–2389.
- [2] N. V. Plechkova, K. R. Seddon, *Methods and Reagents for Green Chemistry*, Wiley, **2007**, pp. 103–130.
- [3] T. Wang, K. J. Jens, *Energy Procedia* **2014**, *51*, 259–266.
- [4] T. J. Wooster, K. M. Johanson, K. J. Fraser, D. R. MacFarlane, J. L. Scott, *Green Chem.* **2006**, *8*, 691–696.
- [5] R. D. Rogers, K. R. Seddon, S. Volkov, *Green Industrial Applications of Ionic Liquids*, Springer, Dordrecht, **2002**.
- [6] R. Gusain, A. Khan, O. P. Khatri, *J. Mol. Liq.* **2020**, *301*, 112322.
- [7] J. Flieger, J. Feder-Kubis, M. Tatarczak-Michalewska, *Int. J. Mol. Sci.* **2020**, *21*, 1–39.
- [8] N. V. Plechkova, K. R. Seddon, *Chem. Soc. Rev.* **2008**, *37*, 123–150.
- [9] T. Itoh, S. Han, Y. Matsushita, S. Hayase, *Green Chem.* **2004**, *6*, 437–439.
- [10] M. J. Earle, K. R. Seddon, *Pure Appl. Chem.* **2000**, *72*, 1391–1398.
- [11] R. Rogers, K. Seddon, *Science* **2003**, *302*, 792–793.
- [12] L. A. Blanchard, Z. Gu, J. F. Brennecke, *J. Phys. Chem. B* **2001**, *105*, 2437–2444.
- [13] E. D. Bates, R. D. Mayton, I. Ntai, J. H. Davis, *J. Am. Chem. Soc.* **2002**, *124*, 926–927.
- [14] T. Wang, K. J. Jens, *Energy Procedia* **2014**, *51*, 259–266.
- [15] S. Seo, M. Quiroz-Guzman, M. A. Desilva, T. B. Lee, Y. Huang, B. F. Goodrich, W. F. Schneider, J. F. Brennecke, *J. Phys. Chem. B* **2014**, *118*, 5740–5751.
- [16] S. Seo, M. A. Desilva, H. Xia, J. F. Brennecke, *J. Phys. Chem. B* **2015**, *119*, 11807–11814.
- [17] S. Seo, M. A. Desilva, J. F. Brennecke, *J. Phys. Chem. B* **2014**, *118*, 14870–14879.
- [18] B. E. Gurkan, J. C. De Fuente, E. M. Mindrup, L. E. Ficke, B. F. Goodrich, E. A. Price, W. F. Schneider, J. F. Brennecke, *J. Am. Chem. Soc.* **2010**, *132*, 2116–2117.
- [19] B. E. Gurkan, T. R. Gohndrone, M. J. McCreedy, J. F. Brennecke, *Phys. Chem. Chem. Phys.* **2013**, *15*, 7796–7811.
- [20] B. Gurkan, B. F. Goodrich, E. M. Mindrup, L. E. Ficke, M. Massel, S. Seo, T. P. Senftle, H. Wu, M. F. Glaser, J. K. Shah, E. J. Maginn, J. F. Brennecke, W. F. Schneider, *J. Phys. Chem. Lett.* **2010**, *1*, 3494–3499.
- [21] C. Wang, H. Luo, D. Jiang, H. Li, S. Dai, *Angew. Chem. Int. Ed.* **2010**, *49*, 5978–5981; *Angew. Chem.* **2010**, *122*, 6114–6117.
- [22] C. Wang, X. Luo, H. Luo, D. E. Jiang, H. Li, S. Dai, *Angew. Chem. Int. Ed.* **2011**, *50*, 4918–4922; *Angew. Chem.* **2011**, *123*, 5020–5024.
- [23] X. Luo, Y. Guo, F. Ding, H. Zhao, G. Cui, H. Li, C. Wang, *Angew. Chem. Int. Ed.* **2014**, *53*, 7053–7057; *Angew. Chem.* **2014**, *126*, 7173–7177.
- [24] Y. Huang, G. Cui, Y. Zhao, H. Wang, Z. Li, S. Dai, J. Wang, *Angew. Chem. Int. Ed.* **2017**, *56*, 13293–13297; *Angew. Chem.* **2017**, *129*, 13478–13482.
- [25] S. A. Didas, R. Zhu, N. A. Brunelli, D. S. Sholl, C. W. Jones, *J. Phys. Chem. C* **2014**, *118*, 12302–12311.
- [26] E. S. Sanz-Pérez, C. R. Murdock, S. A. Didas, C. W. Jones, *Chem. Rev.* **2016**, *116*, 11840–11876.
- [27] F. Vega, A. Sanna, B. Navarrete, M. M. Maroto-Valer, V. Cortes, *Greenh. Gases: Sci. Technol.* **2014**, *4*, 707–733.
- [28] X. Suo, Z. Yang, Y. Fu, C. L. Do-Thanh, D. Maltsev, H. Luo, S. M. Mahurin, D. en Jiang, H. Xing, S. Dai, *ChemSusChem*. **2022**, *15*, e202102136.
- [29] S. Tsubaki, K. Furusawa, H. Yamada, T. Kato, T. Higashii, S. Fujii, Y. Wada, *ACS Sustainable Chem. Eng.* **2020**, *8*, 13593–13599.
- [30] F. Bougie, X. Fan, *Int. J. Greenhouse Gas Control* **2018**, *79*, 165–172.
- [31] T. Chronopoulos, Y. Fernandez-Diez, M. M. Maroto-Valer, R. Ocone, D. A. Reay, *Microporous Mesoporous Mater.* **2014**, *197*, 288–290.
- [32] J. Yang, H. Y. Tan, Q. X. Low, B. P. Binks, J. M. Chin, *J. Mater. Chem. A* **2015**, *3*, 6440–6446.
- [33] P. A. Webley, J. Zhang, *Adsorption* **2014**, *20*, 201–210.
- [34] B. Quan, X. Liang, G. Ji, Y. Cheng, W. Liu, J. Ma, Y. Zhang, D. Li, G. Xu, *J. Alloys Compd.* **2017**, *728*, 1065–1075.
- [35] D. M. P. Mingos, D. R. Baghurst, *Chem. Soc. Rev.* **1991**, *20*, 1–47.

- [36] Y. Y. Lee, B. Gurkan, *J. Membr. Sci.* **2021**, *638*, 119652.
- [37] Y. Y. Lee, D. Penley, A. Klemm, W. Dean, B. Gurkan, *ACS Sustainable Chem. Eng.* **2021**, *9*, 1090–1098.
- [38] Y. Y. Lee, K. Edgehouse, A. Klemm, H. Mao, E. Pentzer, B. Gurkan, *ACS Appl. Mater. Interfaces* **2020**, *12*, 19184–19193.
- [39] H. L. Ngo, K. LeCompte, L. Hargens, A. B. McEwen, *Thermochim. Acta* **2000**, *357 (358)*, 97–102.
- [40] P. Stepnowski, A. Zaleska, *J. Photochem. Photobiol. Chem. A* **2005**, *170*, 45–50.
- [41] N. Banić, B. Abramović, F. Šibul, D. Orčić, M. Watson, M. Vraneš, S. Gadžurić, *RSC Adv.* **2016**, *6*, 52826–52837.
- [42] Y. Huang, Z. Chen, J. M. Crosthwaite, S. N. V. K. Aki, J. F. Brennecke, *J. Chem. Thermodyn.* **2021**, *161*, 106560.
- [43] A. Meißner, A. Efimova, P. Schmidt, *Thermochim. Acta.* **2021**, *704*, 178917.
- [44] K. J. Baranyai, G. B. Deacon, D. R. MacFarlane, J. M. Pringle, J. L. Scott, *Aust. J. Chem.* **2004**, *57*, 145–147.
- [45] M. L. Williams, J. S. Dickmann, M. E. McCorkill, J. C. Hassler, E. Kiran, *Thermochim. Acta.* **2020**, *685*, 178509.
- [46] I. Minami, H. Kamimura, S. Mori, *STLE - 62nd Annual Meeting of the STLE* **2007**, *2*, 135–147.
- [47] O. U. Ahmed, F. S. Mjalli, T. Al-Wahaibi, Y. Al-Wahaibi, I. M. Alnashef, *Ind. Eng. Chem. Res.* **2015**, *54*, 2074–2080.
- [48] T. Yoshida, A. Kawai, D. C. Khara, A. Samanta, *J. Phys. Chem. B* **2015**, *119*, 6696–6702.
- [49] H. Long, B. Pivovar, *J. Phys. Chem. C* **2014**, *118*, 9880–9888.
- [50] S. Sowmiah, V. Srinivasadesikan, M. C. Tseng, Y. H. Chu, *Molecules* **2009**, *14*, 3780–3813.
- [51] K. M. Hugar, H. A. Kostalik, G. W. Coates, *J. Am. Chem. Soc.* **2015**, *137*, 8730–8737.
- [52] S. C. Price, K. S. Williams, F. L. Beyer, *ACS Macro Lett.* **2014**, *3*, 160–165.
- [53] O. D. Thomas, K. J. W. Y. Soo, T. J. Peckham, M. P. Kulkarni, S. Holdcroft, *J. Am. Chem. Soc.* **2012**, *134*, 10753–10756.
- [54] W. Wang, S. Wang, X. Xie, Y. Lv, V. Ramani, *Int. J. Hydrogen Energy* **2014**, *39*, 14355–14361.
- [55] H. Dong, F. Gu, M. Li, B. Lin, Z. Si, T. Hou, F. Yan, S.-T. Lee, Y. Li, *ChemPhysChem* **2014**, *15*, 3006–3014.
- [56] S. Li, M. R. Cerón, H. V. Eshelman, A. J. Varni, A. Maiti, S. Akhade, S. H. Pang, *ChemSusChem.* **2022**, *16*, e202201908.
- [57] G. P. Gardini, *Adv. Heterocycl. Chem.* **1973**, *15*, 67–98.
- [58] V. Bocchi, L. Chierici, G. P. Gardini, *Tetrahedron* **1967**, *23*, 737–740.
- [59] J. K. Howard, K. J. Rihak, A. C. Bissember, J. A. Smith, *Chem. Asian J.* **2016**, *11*, 155–167.
- [60] Y. Tan, K. Ghandi, *Synth. Met.* **2013**, *175*, 183–191.
- [61] A. Holewinski, M. A. Sakwa-Novak, C. W. Jones, *J. Am. Chem. Soc.* **2015**, *137*, 11749–11759.
- [62] J. N. Apell, N. C. Pflug, K. McNeill, *Environ. Sci. Technol.* **2019**, *53*, 11240–11250.
- [63] P. C. Mishra, A. K. Singh, S. Suhai, *Int. J. Quantum Chem.* **2005**, *102*, 282–301.
- [64] S. J. Hawkins, N. M. Ratcliffe, *J. Mater. Chem.* **2000**, *10*, 2057–2062.
- [65] S. Taniguchi, H. Hasegawa, S. Yanagiya, Y. Tabeta, Y. Nakano, M. Takahashi, *Tetrahedron* **2001**, *57*, 2103–2108.
- [66] J. Lacroix, F. Maurel, P. Lacaze, *J. Am. Chem. Soc.* **2001**, *123*, 1989–1996.
- [67] M. Holzweber, R. Lungwitz, D. Doerfler, S. Spange, M. Koel, H. Hutter, W. Linert, *Chem. Eur. J.* **2013**, *19*, 288–293.
- [68] J. E. Gordon, *J. Org. Chem.* **1965**, *30*, 2760–2763.
- [69] M. Schmeisser, P. Illner, R. Puchta, A. Zahl, R. van Eldik, *Chem. Eur. J.* **2012**, *18*, 10969–10982.
- [70] S. J. McGurk, C. F. Martin, S. Brandani, M. B. Sweatman, X. Fan, *Appl. Energy* **2017**, *192*, 126–133.
- [71] A. P. Hallenbeck, J. R. Kitchin, *Ind. Eng. Chem. Res.* **2013**, *52*, 10788–10794.
- [72] Q. Yu, J. D. L. P. Delgado, R. Veneman, D. W. F. Brilman, *Ind. Eng. Chem. Res.* **2017**, *56*, 3259–3269.

Manuscript received: January 25, 2023
Revised manuscript received: March 3, 2023
Accepted manuscript online: March 13, 2023
Version of record online: May 5, 2023